Q. J. R. Meteorol. Soc. (2004), **130**, pp. 3339–3364 doi: 10.1256/qj.03.122

The diurnal cycle of shallow cumulus clouds over land: A single-column model intercomparison study

By GEERT LENDERINK[1]*, A. PIER SIEBESMA[1], SYLVAIN CHEINET[2], SARAH IRONS[3], COLIN G. JONES[4], PASCAL MARQUET[5], FRANK MÜLLER[6], DOLORES OLMEDA[7], JAVIER CALVO[7], ENRIQUE SÁNCHEZ[7] and PEDRO M. M. SOARES[8,9]

[1]*Royal Netherlands Meteorological Institute, De Bilt, The Netherlands*
[2]*Laboratoire de Météorologie Dynamique, Paris, France*
[3]*Met Office, Exeter, UK*
[4]*Swedish Meteorological and Hydrological Institute, Norrköping, Sweden*
[5]*Météo-France, Toulouse, France*
[6]*Max-Planck-Institut für Meteorologie, Hamburg, Germany*
[7]*Instituto Nacional de Meteorologia, Madrid, Spain*
[8]*Instituto Superior de Engenharia de Lisboa, Portugal*
[9]*Universidade de Lisboa, Portugal*

(Received 14 July 2003; revised 11 February 2004)

SUMMARY

An intercomparison study for single-column models (SCMs) of the diurnal cycle of shallow cumulus convection is reported. The case, based on measurements at the Atmospheric Radiation Measurement program Southern Great Plains site on 21 June 1997, has been used in a large-eddy simulation intercomparison study before. Results of the SCMs reveal the following general deficiencies: too large values of cloud cover and cloud liquid water, unrealistic thermodynamic profiles, and high amounts of numerical noise. Results are also strongly dependent on vertical resolution.

These results are analysed in terms of the behaviour of the different parametrization schemes involved: the convection scheme, the turbulence scheme, and the cloud scheme. In general the behaviour of the SCMs can be grouped in two different classes: one class with too strong mixing by the turbulence scheme, the other class with too strong activity by the convection scheme. The coupling between (subcloud) turbulence and the convection scheme plays a crucial role. Finally, (in part) motivated by these results several models have been successfully updated with new parametrization schemes and/or their present schemes have been successfully modified.

KEYWORDS: Boundary-layer Convection EUROCS Large-eddy simulation

1. INTRODUCTION

The representation of clouds in present atmospheric general-circulation models (AGCMs) used in climate research and in numerical weather prediction (NWP) is relatively poor, thereby limiting the predictability of cloud feedbacks in a changing climate. In particular, the representation of shallow cumulus (Cu) convection is an important issue. Shallow cumulus clouds are an integral part of the Hadley circulation, increasing the near-surface transport of moisture to the inter-tropical convergence zone (ITCZ), thereby intensifying deep convection (Tiedtke 1989). Over land, shallow cumulus convection also plays an important role in the preconditioning for deep convection.

For these reasons shallow cumulus convection has been the subject of many studies, in particular by Working Group 1 (WG-1) of GCSS (GEWEX (Global Energy Water cycle EXperiment) Cloud-System Study (Browning 1993)). In the fourth GCSS WG-1 intercomparison case (BOMEX—Barbados Oceanographic and Meteorological Experiment), a typical trade-wind shallow cumulus cloud with low cloud fraction was studied (Siebesma *et al.* 2003). The next case (ATEX—Atlantic Trade-wind Experiment) concentrated on cumulus clouds rising into stratocumulus (Stevens *et al.* 2001), which is

* Corresponding author: Royal Netherlands Meteorological Institute, De Bilt, 3730 AE, The Netherlands.
e-mail: lenderin@knmi.nl

a common cloud regime in the trade-wind area near the transition from stratocumulus clouds to cumulus clouds (de Roode and Duynkerke 1997). Finally, the sixth GCSS WG-1 case (ARM—Atmospheric Radiation Measurement) focused on the diurnal cycle of cumulus clouds over land (Brown *et al.* 2002).

In all these intercomparisons, the main emphasis was on the comparison of large-eddy simulation (LES) results with observations, and the intercomparison of the different LES results. This has been extremely helpful in evaluating the different LES models, giving confidence that LES can be used for these cases as a 'substitute' (but not replacement) for reality, providing us with a full three-dimensional (3D) picture of the turbulent motions where measurements are sparse. This also opens a way to evaluate critically the different parametrizations involved with the representation of convective clouds like, for example, mass-flux schemes and cloud schemes. In particular, the BOMEX case has been very popular in this respect (e.g. Siebesma and Cuijpers 1995; Siebesma and Holtslag 1996; Grant and Brown 1999; Bechtold *et al.* 2001; van Salzen and McFarlane 2002; Neggers *et al.* 2002).

Despite this, relatively little attention has been paid to the critical evaluation and documentation of results from single-column models (SCMs) derived from (semi-) operational NWP or climate models. In the last few years, however, it has become clear that this step is essential, and that the whole cycle of intercomparing observations, LESs and SCMs (and full 3D AGCM simulations) is critical to actually improving parametrizations in operational models.

This paper studies the representation of the diurnal cycle of cumulus convection in several SCM versions of (semi-) operational models. We use the GCSS WG-1 sixth case studying the diurnal cycle of cumulus clouds (Brown *et al.* 2002) for the following reason. This case is rather demanding because all the parametrizations in the SCM have to work together in the different regimes capturing the diurnal cycle. What might work well in the mature stage of Cu clouds might not work properly in other stages of the diurnal cycle. Further, many of the parametrizations recently developed have been tuned to the stationary marine BOMEX case, and it is not clear how well they work for this non-stationary continental case.

The first objective of the paper is to show how realistic cumulus clouds are represented by state-of-the-art operational climate/NWP models. The models considered are: ARPEGE (CLIMAT), ECHAM4, the ECMWF model (hereafter shortly denoted ECMWF), HIRLAM, MESO-NH, RACMO and the Met Office model (hereafter METO). These models are described in the appendix (see also Table A.1). The second objective is to analyse the behaviour of the different parametrization schemes involved. These are the turbulence scheme, the convection scheme and the cloud/condensation scheme. We keep this analysis as general as possible, not focusing too much on the behaviour of one particular model, but attempting to identify typical behaviour in classes of models/or parametrizations. In this respect, it is explicitly mentioned that it is not our purpose to distinguish between *good* and *bad* models. One bad assumption or bad scheme might jeopardize the solution of an otherwise good model, and relatively good results might be obtained through cancelling errors. As part of the analysis we also show some results of research models, that are not (yet) in operational use, in order to illuminate our findings further. Finally, (in part) motivated by these results, several models have been successfully updated with new parametrization schemes and/or their present schemes have been successfully modified. The outcome of these improvements is also documented here. This comparison is part of the European Union funded EUROCS (European Cloud Systems) project, which aims at improving the representation of clouds in climate models.

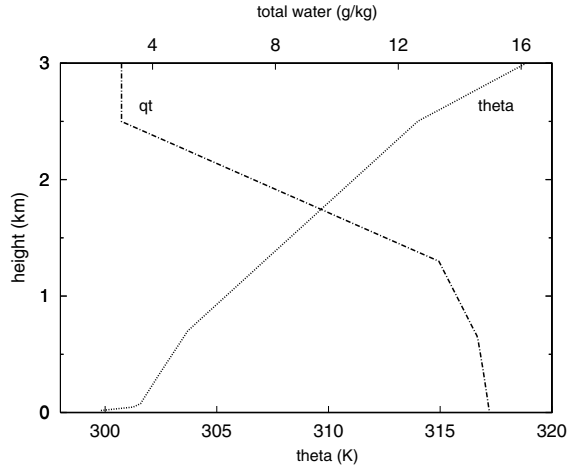

Figure 1. Initial profiles of potential temperature θ (K) (dotted line) and total water q_t (g kg^{-1}) (dot-dashed line).

2. CASE

(*a*) *Case description*

The case is based on an idealization of observations made at the ARM Southern Great Plains (SGP) site on 21 June 1997. During that day cumulus clouds developed on top of a clear convective boundary layer. The case was compiled by Andy Brown of the Met Office and has been described in detail by Brown *et al.* (2002).

The initial profiles are shown in Fig. 1. The surface latent- and sensible-heat fluxes are prescribed, with values close to zero in early morning and the evening, and a maximum at midday of 500 W m^{-2} and 140 W m^{-2}, respectively. This implies a Bowen ratio of approximately 0.3, whereas typical values in marine Cu are much lower (e.g. 0.06 in BOMEX). Small tendencies representing the effect of large-scale advection and short-wave radiation are prescribed (for details see Brown *et al.* (2002)).

(*b*) *Summary of LES results*

Brown *et al.* (2002) discussed the results of eight LES models. The spread between these different LES results was relatively small, in particular in comparison with the spread in the SCM results presented here. For convenience we therefore only present LES results of the KNMI* LES model (Cuijpers and Duynkerke 1993).

In Fig. 2 the evolution of the potential temperature and the cloud liquid water in the LES is shown. The evolution of the potential temperature reveals the growth of the inversion from near the surface to 800 m at 1500 UTC (0900 local time) when clouds appear. At that time clouds are shallow with the highest cloud tops at 1000–1500 m, but gradually the cloud layer deepens with the highest cloud tops at 2500–2800 m after 1900 UTC (1300 local time). At the same time cloud base rises from 800 m to 1300 m. Values of cloud liquid water (domain averaged) are relatively low with values of 0.01–0.04 g kg^{-1}.

Other LES results are shown in concert with the SCM results. We focus mainly on time-series of liquid-water path (LWP) and cloud fraction, and on the vertical profiles at

* Royal Netherlands Meteorological Institute.

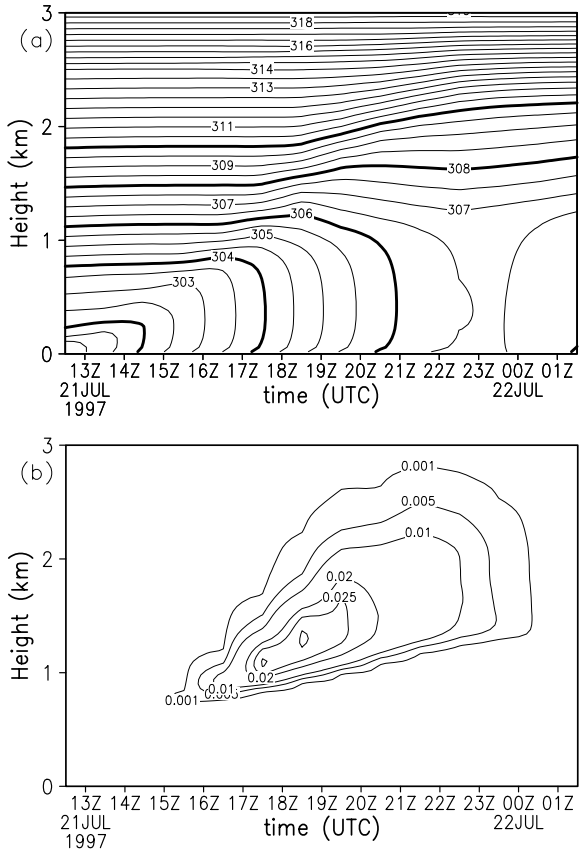

Figure 2. Time evolution of (a) the potential temperature and (b) the cloud liquid water in the KNMI large-eddy simulation model. The contour intervals are 1 K and 0.005 g kg^{-1}, respectively, with an additional contour at 0.001 g kg^{-1}.

two different stages: at 1730 UTC with a shallow cloud layer forced from the subcloud, and at 2130 UTC with well developed active clouds.

3. Results of the (semi-) operational versions

We intercompare results of seven different models: ARPEGE (CLIMAT), ECHAM4, ECMWF, HIRLAM, METO, MESO-NH and RACMO. For METO only the mean profiles and the time-series were available. These models and their physics packages are described briefly in the appendix. Some relevant model aspects are also described in concert with the analysis of the results.

Most participants have run their models on two different vertical resolutions, R_{19} and R_{40} with, respectively, 19 and 40 levels in the lowest 4 km of the atmosphere. Resolution R_{19} equals (in the lowest 4 km) the L60 resolution presently operational at ECMWF (Teixeira 1999). R_{19} has a vertical grid spacing of 200–400 m in the cloud layer (and higher near the surface). Even though R_{19} is, at present, a high operational resolution, the cloud layer is only resolved by three or four points and the numerical errors are relative large. Therefore, we also requested R_{40} with a grid spacing of 150–200 m in the cloud layer. If available, we therefore show results on R_{40}. For ECMWF and HIRLAM we show results on R_{19}, since results on R_{40} were not available. It is

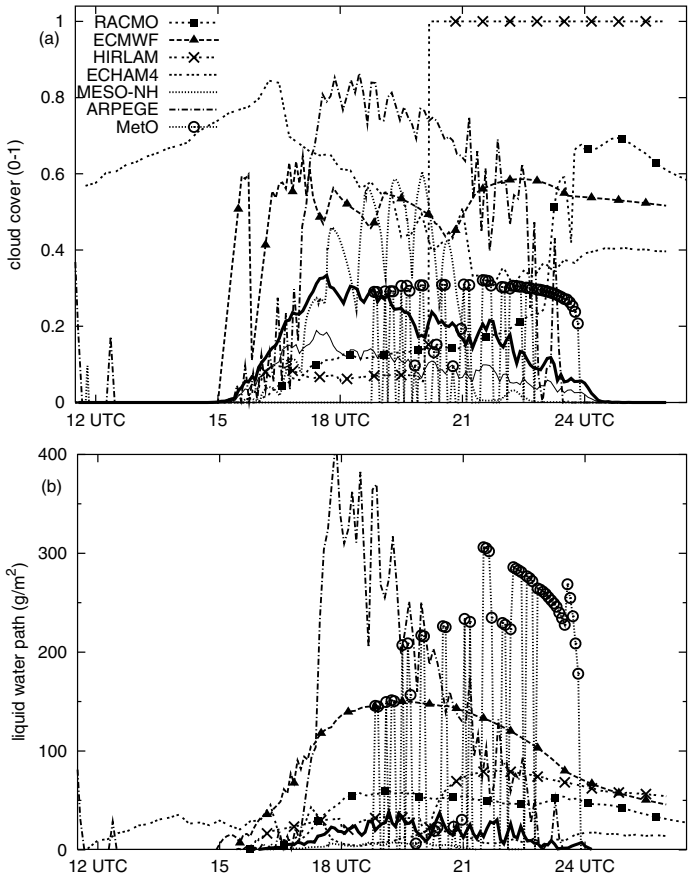

Figure 3. Time-series of (a) cloud cover (0–1) and (b) cloud liquid-water path (g m^{-2}) in different models (see Table A.1). The large-eddy-simulation (LES) results for total cloud cover are shown by the thick solid line and the maximum cloud fraction by the thin line.

noted here that in ECHAM4 and METO, the results on R_{40} are rather different from those at the lower vertical resolution at which the model is run operationally. Sensitivity to vertical resolution is shown in section 5(*c*).

(*a*) *Time-series*

In Fig. 3, the time evolution of the total (projected) cloud cover is shown. Most models have too high a cloud cover in the mid-afternoon, over 50% in ECMWF, ECHAM4, ARPEGE and HIRLAM. In addition, in most models, clouds do not dissolve at the end of the day (HIRLAM, RACMO, ECMWF, ECHAM4), or even peak in cloud fraction after sunset (RACMO and HIRLAM). ECHAM4 already has a rather high cloud cover in the early hours of the simulation.

It is not entirely trivial to compare total projected cloud cover in the SCMs and in the LES. Both the LES and SCMs predict a cloud fraction at each model height (see, for example, Fig. 5). The total cloud cover is defined as the vertical projection of the 3D cloud field onto the surface. Because in the LES the full 3D cloud field is available, the projected cloud cover can be computed; in the LES the projected cloud cover is a factor of two larger than the maximum of the cloud fraction profile. However, in the

SCMs a full 3D cloud field is not available and a cloud-overlap assumption has to be made. With the common assumption of maximum random overlap and the LES profile in Fig. 5, the projected cloud cover would equal the maximum of the cloud-fraction profile, and the cloud cover would, therefore, be underestimated. On the other hand, ARPEGE produces a cloud cover far exceeding the maximum of the cloud-fraction profile (in Fig. 5) since the cloud-overlap assumption effectively treats the different maxima in the cloud-fraction profile as separate (independent) cloud layers.

The cloud LWP (the vertical integral of the mean liquid-water content) shows similar behaviour. Most SCMs have LWPs that are a factor two to five times higher than in the LES model, the most extreme being in ARPEGE and METO with values over 300 g m^{-2}, and in ECMWF reaching 150 g m^{-2}. In LWP, as in the cloud cover, most SCMs show a high level of intermittency. Note that the intermittency in the LES results is caused by sampling of a relatively small amount of clouds in the LES domain of 6.4×6.4 km^2. Most SCMs, however, are representative for (much) larger domain sizes, and the parametrizations do not explicitly represent the life-cycle of a single cloud and, therefore, should not contain this type of intermittency.

(*b*) *Profiles*

Profiles at 1730 UTC, just after the onset of clouds, are shown in Fig. 4. In the LES model, there is a shallow cloud layer with cloud base at 800 m and highest cloud tops at 1500 m. There is no well-developed conditionally unstable profile yet, as can be seen in the (mean) profiles of total water, q_t, and the potential temperature, θ, (which, in this case, is close to the liquid-water potential temperature, θ_l, since the cloud liquid-water content is small). In this phase, the clouds are mainly forced from the subcloud layer. The profiles of θ and q_t in the SCMs are reasonably close to the LES results. Some SCMs, however, developed a considerable amount of grid-point noise, in particular in ECHAM4 (see, for example, the results for q_t, relative humidity and horizontal velocity, u). At this early stage of cloud formation, the cloud fraction and cloud liquid water already show rather high values in most SCMs (except in HIRLAM, and METO which has no clouds at this time). In the LES model, the shape of profiles of liquid water and cloud fraction is similar but, in the SCMs, they are often rather dissimilar. For example, ECHAM4 has clouds reaching the surface, but no correspond liquid water, and in ECMWF the liquid water strongly peaks at one layer in the inversion, but the cloud layer extends over more layers. MESO-NH has a rather high cloud fraction (45%) but almost no corresponding liquid water. RACMO shows the opposite behaviour, with somewhat low cloud fractions, but too much cloud liquid water. ECHAM4 and RACMO have unrealistic wind profiles with a strong minimum in u in the cloud layer. ECMWF has too strong winds in the subcloud layer.

The profiles at 2130 UTC (1530 local time) are shown in Fig. 5. The differences between the LES model and the SCMs, and between different SCMs, have increased significantly. Four models (ECMWF, ARPEGE, ECHAM4, and METO) have high moisture contents near the inversion above 2000 m, whereas the lower part of the cloud layer, in particular near cloud base, is too dry. ECMWF and ECHAM4 are too warm in the lower part of the cloud layer, with a (strong) inversion at cloud base. On the other hand, the profiles of potential temperature in ARPEGE and METO are too well-mixed in the cloud layer. HIRLAM is characterized by a very shallow boundary layer, which is too moist and covered with thick stratiform clouds. The temperature and moisture profiles in RACMO and MESO-NH are reasonably close to the LES results (see, for example, the profile of relative humidity), but the cloud fraction in MESO-NH is too small and the cloud liquid water in RACMO too large. ECMWF has a remarkable peak in cloud

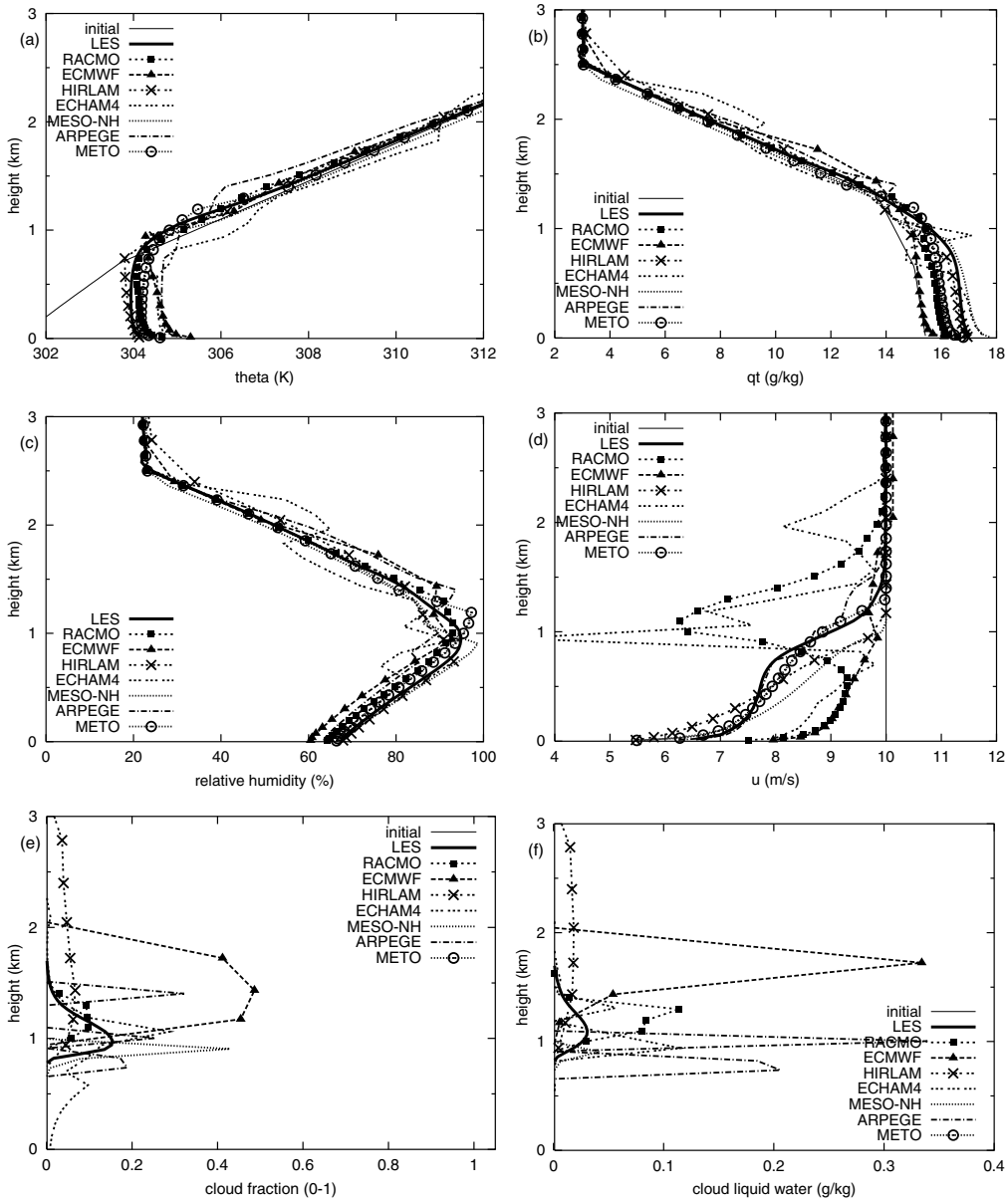

Figure 4. Profiles of (a) potential temperature θ (K), (b) total water q_t (g kg^{-1}), (c) relative humidity (%), (d) horizontal velocity u (ms^{-1}), (e) cloud fraction and (f) cloud liquid water q_l (g kg^{-1}) for different models (see Table A.1) at 1730 UTC (1130 local time)—the large-eddy simulation results are hourly averages and the single-column model results are instantaneous values. The thin solid lines denote the initial profiles.

fraction in the inversion, despite the fact that the relative humidity at that height is below 80%. A peak in cloud fraction in ARPEGE at 2500 m corresponds to a maximum in relative humidity (90%) at that height. Noise is apparent in the profiles of ECHAM4 and, to a lesser extent, in ARPEGE. Note that, for example, ECHAM4 seems to have problems with conserving heat, or perhaps did not apply the correct forcing, since it is too warm (compared with LES) everywhere.

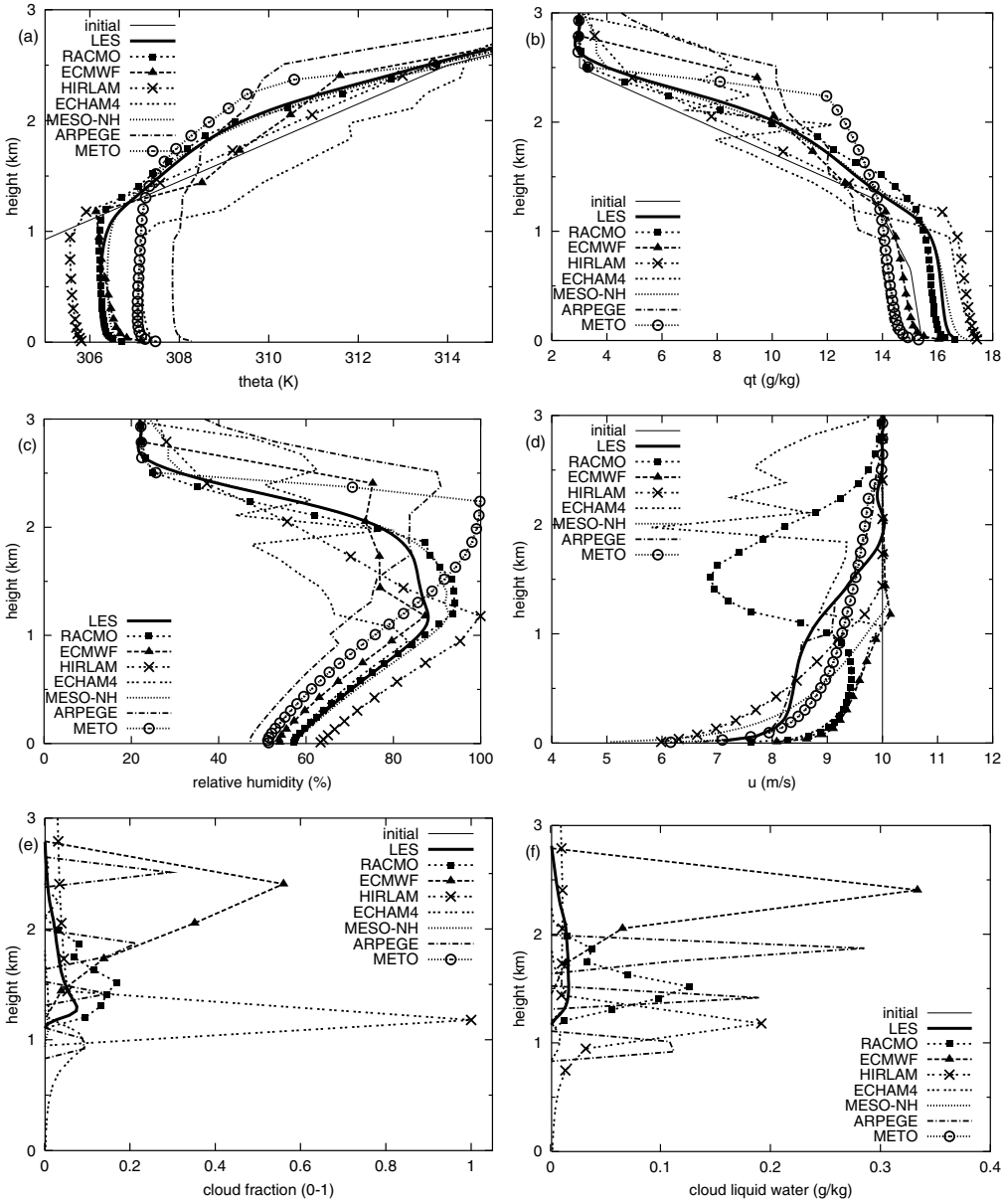

Figure 5. As Fig. 4 but at 2130 UTC (1530 local time). Note that these are instantaneous values. In models with intermittent behaviour this may be rather different from the time-averaged results. For example, METO has no cloud at this time, whereas from the time-series it is clear that there are clouds in the time-mean values.

In four models the clouds did not dissolve at the end of the day. Figure 6 shows the relative humidity and cloud fraction in the evening (1930 local time) at a time when the cloud should have disappeared. RACMO and HIRLAM are close to saturation just below the inversion, and accordingly predict high cloud fractions. In ECMWF the cloud fraction peaks close to the inversion at a higher level. In ECHAM4 some thin clouds remain, despite the comparatively low relative humidity.

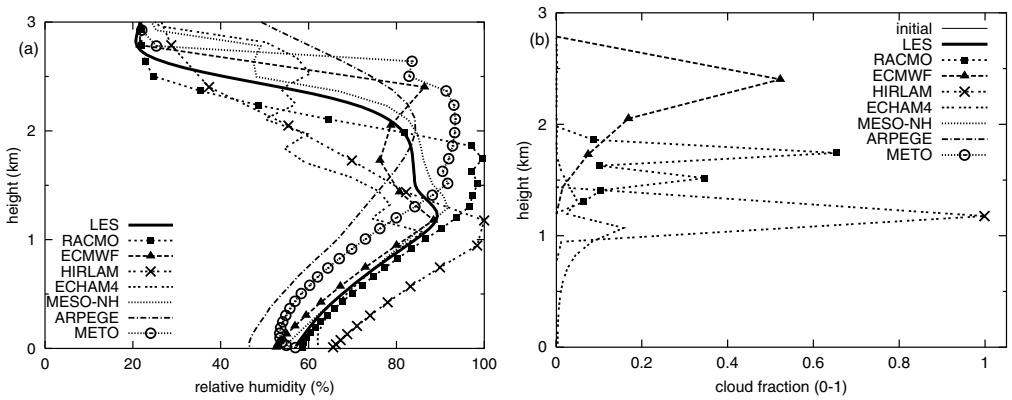

Figure 6. Profiles of (a) relative humidity and (b) cloud fraction for different models (see Table A.1) at 0130 UTC (1930 local time).

4. Analysis of the results

The results are analysed in terms of the individual behaviour of the different parametrization schemes and their mutual interaction. As discussed in the introduction, three parametrizations play a major role: (1) the turbulence scheme, (2) the convection scheme, and (3) the cloud/condensation scheme.

(*a*) *Turbulence*

All models use diffusion to represent subcloud turbulent mixing; that is, the turbulence scheme computes fluxes from

$$\overline{w'\phi'}_{\text{turb}} = -K_\phi \frac{\partial \phi}{\partial z}, \tag{1}$$

where $\phi = \{u, v, \theta, q, \text{etc.}\}$. Here, and in the following, ϕ denotes the grid-box mean value. Commonly used closures to compute the eddy diffusivity, K, are the TKE-l closure, the Louis (1979) closure, or the K-profile method (Troen and Mahrt 1986). Except METO, none of the models use a non-local transport term (such as, for example, the scheme proposed by Holtslag and Boville (1993)).

The TKE-l scheme employs a prognostic equation for turbulent kinetic energy (TKE or E) combined with a diagnostic length scale:

$$K = l_{\text{turb}}\sqrt{E}. \tag{2}$$

Different TKE-l schemes use rather different rules to prescribe the length scale, l_{turb}, in terms of local and/or non-local stability measures: e.g. based on a parcel method in MESO-NH (Bougeault and Lacarrère 1989) or based on the local Richardson number, Ri, in ECHAM4 (Roeckner *et al.* 1996). The Louis (1979) closure uses

$$K = l_{\text{turb}}^2 \left| \frac{\partial \overline{\mathbf{U}}}{\partial z} \right|, \tag{3}$$

with l_{turb} depending on Ri and chosen such that, near the surface, the scheme matches the surface flux-profile relations. The K-profile method (Troen and Mahrt 1986) uses prescribed approximately-quadratic profiles from the surface to the top of the convective

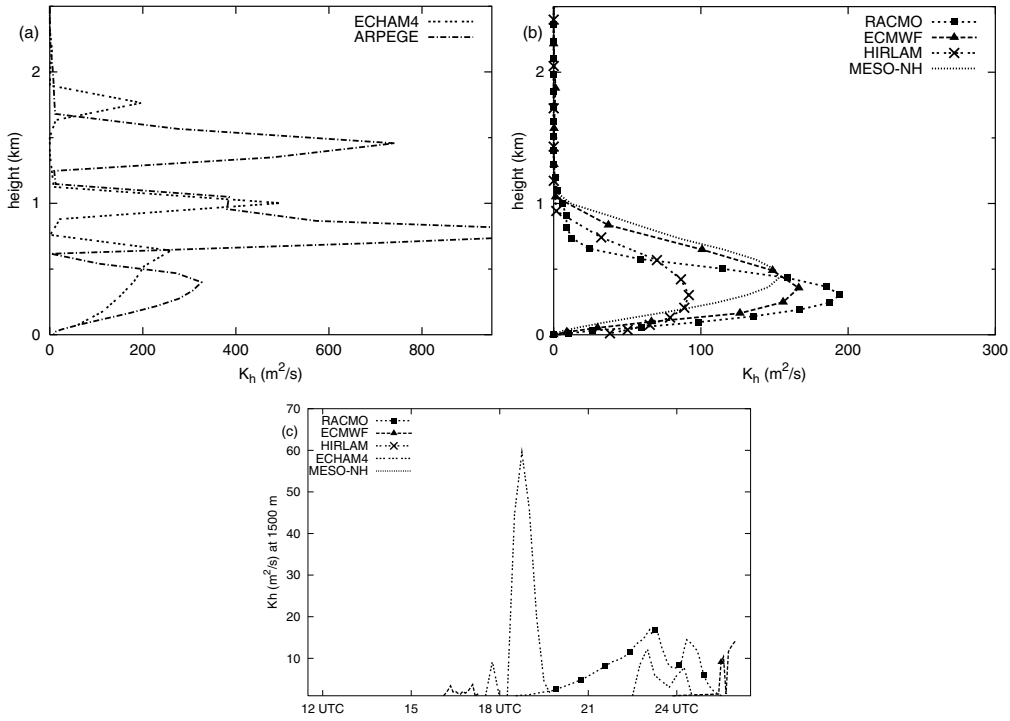

Figure 7. Profiles of K_h at 1730 UTC for (a) ECHAM4 and ARPEGE, (b) RACMO, ECMWF, HIRLAM, and MESO-NH, and (c) the time-series of K_h in the cloud layer at 1500 m (m^2s^{-1}).

boundary layer. In such a scheme, the entrainment flux at the boundary-layer top is often prescribed.

ECMWF and METO use a K-profile method with prescribed entrainment rate, and ARPEGE uses the second-order scheme of Mellor and Yamada (1974) based on diagnostic (instead of prognostic) TKE. For stable conditions ECMWF uses the Louis (1979) closure. The other models use a TKE-l scheme, but with rather different formulations of the length scale.

The profiles of the eddy diffusivity for heat K_h at 1730 UTC are shown in Fig. 7. In the cloud layer, ARPEGE and ECHAM4 have profiles that are spatially incoherent, with spikes up to unrealistically high values of 500–1000 m^2s^{-1} (Fig. 7(a)). All other models have rather similar 'quadratic' shapes for K_h, but with rather different maximum values ranging from 100 to 300 m^2s^{-1}. Usually this maximum is estimated to be the order of $0.1hw_*$ (Holtslag and Moeng 1991), with h the dry convective boundary-layer height and w_* the convective velocity scale. In our case, this gives an estimate of K_h of about 150 m^2s^{-1}. It should be noted that, in practice, there is not such a big difference between a value of 100 and a value of 300 m^2s^{-1}, since the subcloud boundary layer will remain well-mixed in both cases. Also non-local transport terms might play a role; Stevens (2000) showed that the value of K_h and the non-local transport term are related, producing in certain regimes realistic thermodynamic lapse rates. Apart from METO, none of the SCMs considered here have explicit non-local transport terms, and consequently they retain a slightly unstable lapse rate up to the base of the entrainment layer at the top of the dry convective boundary layer.

(*b*) *Moist turbulent mixing*

ECHAM4, RACMO, ARPEGE and MESO-NH have turbulence schemes that represent cloud condensation effects in the computation of the buoyancy fluxes and atmospheric stability. The buoyancy flux can be computed from the fluxes of total-water and liquid-water potential temperature by:

$$\rho c_p \overline{w'\theta'_v}\big|_{u,s} = \alpha_{u,s}\rho c_p \overline{w'\theta'_l} + \beta_{u,s}\rho L \overline{w'q'_t}, \tag{4}$$

where α and β (for exact definitions see, for example, Cuijpers and Duynkerke (1993)) are dependent on whether the atmosphere is unsaturated with no cloud water (subscript 'u') or saturated (subscript 's'). In dry conditions, $\alpha_u = 1$ and $\beta_u \approx 0.07$. With a latent-heat flux of 500 W m^{-2} and a sensible-heat flux of 140 W m^{-2}, the moisture flux amounts to about 30% of the buoyancy flux. In saturated conditions, however, $\alpha_s \approx 0.5$ and $\beta_s \approx 0.4$ which, in this case, means that the moisture flux dominates the buoyancy flux for saturated conditions. The vertical stability is computed from the gradients of q_t and θ_l in a similar way. In partly cloudy conditions, the buoyancy flux is obtained by a linear interpolation in the cloud fraction, a, of the dry and moist contributions:

$$\rho c_p \overline{w'\theta'_v} = (1-a)\rho c_p \overline{w'\theta'_v}\big|_u + a\rho c_p \overline{w'\theta'_v}\big|_s. \tag{5}$$

For skewed motions Eq. (5) can be extended to include the non-Gaussian part (Cuijpers and Bechtold 1995). This is done in MESO-NH and will be done in next version of ARPEGE. This, however, may induce overlap with the convection scheme ('double counting').

In addition, these models (except ARPEGE) use mixing in moist conserved quantities (e.g. in q_t and θ_l) or add separate mixing of cloud liquid water. Although the use of diffusion for cloud liquid water might be questioned, the procedure of mixing liquid and water vapour separately can lead to realistic fluxes of conserved variables—diffusion is a linear operator—in cloudy boundary layers (for a discussion on this subject see, for example Lenderink and van Meijgaard (2001)).

Because the formulation of buoyancy flux given by Eq. (5) is strongly dependent on the cloud fraction, small changes in cloud fraction have a large impact on the atmospheric stability and the buoyancy flux. The dependency in the moist turbulence scheme may give rise to instability (in ARPEGE and ECHAM4) and cloud-regime transitions from Cu to more stratiform clouds (in RACMO), or vice-versa. In ECHAM4 the instability is related to the limit behaviour of the Louis (1979) stability functions for small wind shear in combination with a moist formulation for stability (Lenderink and van Meijgaard 2001; Lenderink *et al.* 2000). In that case, small local variations in cloud fraction strongly impact on the computed atmospheric stability and, therefore, on the length scale and turbulent mixing. The turbulent fluxes again feed back onto cloud fraction by changing humidity and temperature profiles. Potentially, this is a very strong destabilizing feedback loop. The instability in ECHAM4 is visible from the time-series and profiles of K_h in the cloud layer in Fig. 7. In RACMO, a similar feedback gives rise to increasing cloud cover with time. More active mixing in the cloud layer tends to straighten the profiles, giving rise to a shallow, but well mixed, boundary layer representative of stratiform clouds. This positive feedback is, for example, visible in the time-series of K_h in the cloud layer (Fig. 7). In stratiform clouds, long-wave cooling is an important source of turbulence but, in the present case, it is neglected. Taking long-wave cooling into account, we might expect this feedback to have a stronger effect, resulting in still higher cloud fractions.

(*c*) *Convection*

All models except ARPEGE run with an explicit parametrization of convective transports in the cloud. HIRLAM uses an adapted version of the Kuo (1974) scheme; all other models use a bulk mass-flux approach: RACMO, ECHAM4, ECMWF based on Tiedtke (1989); MESO-NH based on Kain and Fritsch (1990) and METO based on Gregory and Rowntree (1990). None of the models explicitly switch off turbulent diffusion when the convection scheme is active, so convective transports and turbulent diffusion may act simultaneously in the cloud layer.

In the following analysis, we concentrate on mass-flux closures, mainly because most recent developments in parametrizations of convection have been achieved in these type of schemes. The bulk mass-flux approach computes the convective fluxes from

$$\overline{w'\phi'}_{\text{conv}} = M(\phi^{\text{up}} - \phi), \tag{6}$$

with the equation for the cloud updraught ϕ^{up}

$$\frac{\partial \phi^{\text{up}}}{\partial z} = \epsilon(\phi - \phi^{\text{up}}) \tag{7}$$

and the mass flux M

$$\frac{\partial M}{\partial z} = (\epsilon - \delta)M. \tag{8}$$

Here, ϵ and δ govern the amount of updraught mass due to entrainment and detrainment, respectively. Mass-flux schemes mainly differ in how the values at cloud base and the fractional entrainment and detrainment coefficients, ϵ and δ, are prescribed. In the inversion, the updraught becomes negatively buoyant, and above the zero-buoyancy level the mass flux detrains massively.

In Fig. 8 we have plotted the flux produced by the mass-flux scheme (as defined by Eq. (6)) for θ_{l} and q_{t}. These fluxes represent a warming and drying near cloud base, and a moistening and cooling close to the inversion. In ECHAM4 and ECMWF this effect is very strong. To analyse this behaviour we focus first on the mass flux M in Fig. 8(c). In the cloud layer, the mass flux in two models (ECMWF and ECHAM4) is constant with height, with massive detrainment in a shallow layer in the inversion. In ECHAM4 it is assumed that 80% of the detrainment takes place in the first layer above the zero-buoyancy level and 20% in the next level. At this high vertical resolution this causes an extremely rapid detrainment. In MESO-NH the mass flux above cloud base first strongly increases, followed by a rapid decrease. RACMO has a gradual decrease in the mass flux fixed by the entrainment and detrainment coefficients in Siebesma and Holtslag (1996).

It should be noted that all model results have linear profiles for the fluxes of total-water and liquid-water potential temperature from the surface to cloud base. This represents transport by the organized flow in the subcloud layer connected to the cumulus cloud, drawing moisture and heat from the subcloud layer. This is part of the closure assumption used in the models. The mass flux, M, is not used in the subcloud layer, and its shape in the subcloud layer is, therefore, irrelevant.

In general, the difference between the updraught and the mean field (not shown) increases with height above cloud base. We illustrate this for moisture by writing Eq. (7) as

$$\frac{\partial \triangle q}{\partial z} + \epsilon \triangle q = \Gamma_q, \tag{9}$$

with $\triangle q \equiv q^{\text{up}} - q$ and $\Gamma_q \equiv -\partial q/\partial z$. If we assume Γ_q and ϵ to be constant, just for the sake of the argument, this equation can solved easily (see also Eq. (A3) in the paper

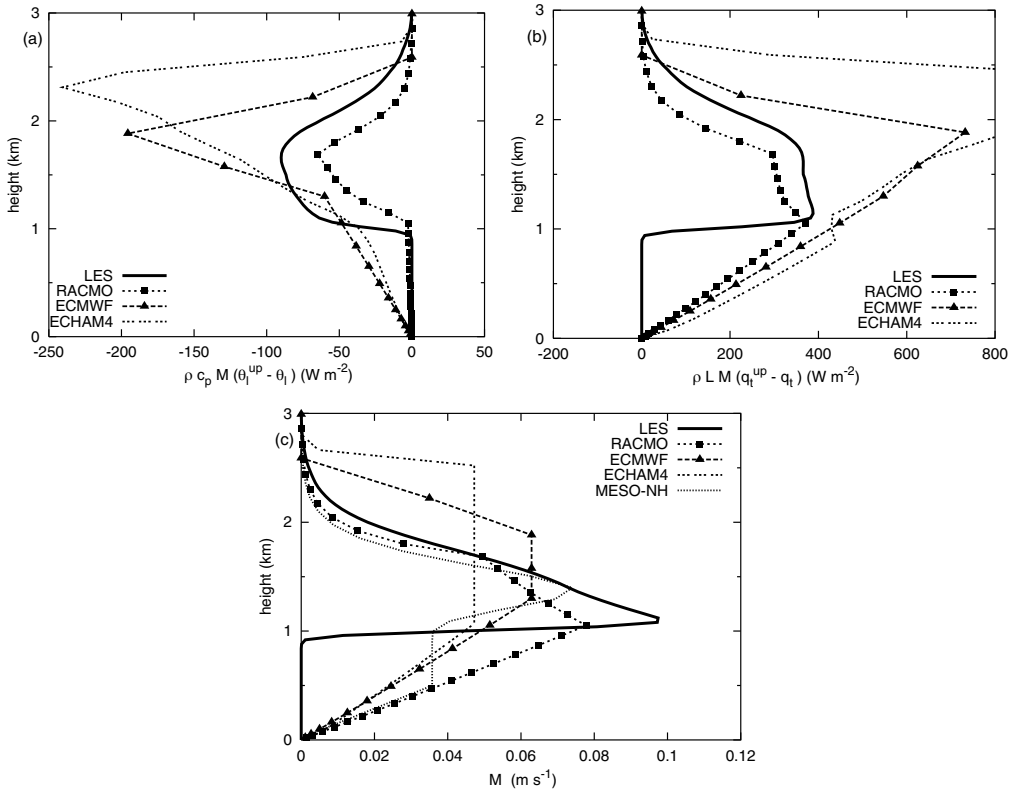

Figure 8. Profiles of fluxes of (a) θ_l and (b) q_t from the mass-flux scheme (W m^{-2}), and (c) the mass flux, M, (m s^{-1}).

by Siebesma and Holtslag (1996))

$$\triangle q = \frac{\Gamma_q}{\epsilon} + \left(\triangle q_{\text{base}} - \frac{\Gamma_q}{\epsilon} \right) \exp\{-\epsilon (z - z_{\text{base}})\}, \tag{10}$$

with $\triangle q_{\text{base}}$ being $\triangle q$ at cloud base, and z_{base} the cloud-base height. The first term is the asymptotic behaviour, and the second term the behaviour near cloud base. Taking typical values of $\triangle q_{\text{base}} \approx 1$ g kg^{-1}, $\Gamma_q \approx 4 \times 10^{-3}$ g kg^{-1}m^{-1} and $\epsilon \approx 2 \times 10^{-3}$, the second term is negative, so $\triangle q$ increases with height above cloud base. Given that, in general, the mass flux in the SCMs is rather constant (or sometimes even increases with height), the flux of the total water increases with height. This reflects that the mass-flux scheme takes away moisture from the lowest part of the cloud and deposits it in, or close to, the inversion. In ECHAM4 and ECMWF this effect is very pronounced (see Fig. 8), which is at odds with the LES results and common sense. Hence, the mass flux should decrease with height in order to obtain moisture fluxes that also decrease with height. Similar arguments hold for the flux of liquid-water potential temperature.

The increase in the convective flux of total water with height is responsible for the large gradient just above cloud base. In the subcloud layer this gradient does not occur because of the intense mixing by the turbulence scheme. In terms of potential temperature, an inversion is created just above the well-mixed subcloud layer. This is clearly visible in the profiles of, especially, relative humidity in Fig. 5 (ECMWF and

ECHAM4). There is a positive feedback because the difference between updraught and mean field increases during this process.

The high moisture content above 2300 m in ECHAM4 and ECMWF are caused by too strong activity of the mass-flux scheme, depositing too much moisture in, or just above, the inversion. In ECMWF, time-series of the mass flux at cloud base revealed that, in the first few hours after the onset of the clouds, the mass flux obtained very high values of 0.2 kg $m^{-2}s^{-1}$. This confirms the results of Neggers *et al.* (2004), where it was shown for this case that the mass-flux closure based on moist static-energy convergence strongly overpredicts the cloud-base mass flux during the early stages of cloud formation.

All models except HIRLAM trigger convection at about the same time, mainly due to the dominance of the strong surface forcing. However, simulations of the diurnal cycle of stratocumulus clouds showed that some of the SCMs did also trigger the mass-flux scheme in that case, which causes a significant reduction of the cloud cover (Duynkerke *et al.* 2004). Moreover, the results shown by Jakob and Siebesma (2003) showed that the triggering function is extremely important in AGCM simulations of ECMWF.

In HIRLAM, a switch turns convection smoothly off when the horizontal grid spacing gets finer. This switch was mainly developed with deep convection in mind, but it acts for shallow convection also. The results presented here are for a horizontal resolution of 4 km, which is the typical resolution that HIRLAM aims at in the near future. Results at a resolution of 20 km (not shown) are better, with much deeper clouds extending to 2500 m during the mid afternoon. But also in this simulation a rather thick low-level cloud develops at the end of the day after 23 UTC.

(*d*) *Interaction of turbulence and convection*

The interaction between the convection scheme and the turbulence scheme plays an important role. Both the turbulence and the mass-flux scheme determine how the profiles of temperature and humidity evolve. The resulting profiles, in particular near cloud base, again influence mass-flux activity and/or turbulent activity, potentially giving rise to strong feedback loops.

In some models, the role of the turbulence scheme is crucial to prevent unrealistically strong drying of the lower part of the cloud layer due to the mass-flux scheme. However, the inversion near cloud base caused by the mass-flux scheme may limit turbulent transports. In this case, a run-away process may occur. Dry turbulence schemes are slightly more susceptible to this feedback, but it may also occur in moist turbulence schemes. In ECHAM4, the stability functions in terms of the local Ri and the limit behaviour for small wind shear (Lenderink and van Meijgaard 2001) are responsible for a cessation of turbulent transports across cloud base.

On the other hand, a feedback between the cloud-base closure of the mass-flux scheme and the turbulence scheme might lead to a reduction of convective activity. This type of feedback may occur with closures based on the assumption of subcloud equilibrium or, more precisely, based on subcloud convergence of moisture (ECHAM4 and RACMO) or moist static energy (ECMWF). In that case, the mass flux at the subcloud layer is adjusted so that the total moisture (or moist static energy) content of the subcloud layer remains constant:

$$M_{\text{base}} = \frac{\overline{w'q'_{\text{t}}}|_{\text{s}} - \overline{w'q'_{\text{t}}}|_{\text{base}}}{(q^{\text{up}} - q)_{\text{base}}}, \tag{11}$$

with $\overline{w'q_t'}|_s$ the surface latent-heat flux and $\overline{w'q_t'}|_{base}$ the moisture flux through cloud base generated in the turbulence scheme. In this closure, the following feedback may occur. If the stability at cloud base weakens, the turbulence fluxes at cloud base will increase. In effect, the closure will reduce the mass-flux activity. This process will erode the inversion at cloud base further (due to combined effects of more active diffusion and less mass-flux activity). Schemes with moist turbulence schemes are more susceptible to this feedback (e.g. in RACMO). Obviously, this feedback is strongly dependent on the type of closure; for example, it does not occur with closures based on the subcloud turbulent velocity scale (Grant 2001), such as is used, for example, in METO.

Since mass-flux schemes are basically advection schemes, the way the advection operator is implemented plays an important role. Many of the present-day operational mass-flux schemes use implementations that are close to upwind differencing (Tiedtke 1989). They introduce considerable amounts of numerical diffusion (with K of order $M\Delta z/2 \approx 1$–$10\ \mathrm{m^2 s^{-1}}$, with Δz the grid spacing). In fact, using a non-diffusive central differencing in ECMWF, large gradients at cloud base occurred. Since, at high resolution, numerical diffusion becomes insignificant, these models tend to become more unstable with increased vertical resolution. In combination with turbulence schemes based on local stability measures (like, for example, Ri) this may give rise to high levels of noise.

(*e*) *Cloud schemes*

There is a large spread in how models treat cloud fraction, cloud liquid water, and evaporation and condensation. The range spans from statistical schemes, which diagnose cloud liquid water and cloud fraction based on mean values of q_t and θ_l and estimates of their subgrid variability (in MESO-NH and ARPEGE), to process-based schemes with prognostic equations for both cloud liquid water and cloud fraction (ECMWF). Other models combine a diagnostic cloud cover, based on relative humidity (HIRLAM, ECHAM4) or total water (RACMO), with a prognostic equation for cloud condensate based on Sundqvist *et al.* (1989). Due to this variety in cloud schemes used, it is hard to draw general conclusions from the results. In addition, the fact that most models drift away from realistic temperature and humidity profiles rather quickly (as is shown in Fig. 5) complicates the analysis. A perfect-model approach in which cloud schemes are fed with realistic mean profiles would be more revealing, but this approach was not exercised here. An example of such an approach has been discussed by Siebesma *et al.* (2003).

One rather general conclusion one might draw from the results is that, in the prognostic schemes, cloud fraction and cloud liquid water are (often) strongly tied to the convective activity. For example, in these models the detrainment of liquid water by the mass-flux scheme is used as a source term for the liquid water, given by:

$$\left(\frac{\partial q_l}{\partial t}\right)_{\mathrm{detr}} = q_l^{\mathrm{up}} \max\left(0, -\frac{\partial M}{\partial z}\right). \tag{12}$$

In several models (ECHAM4, RACMO, and ECMWF) this leads to a peak in cloud liquid-water content close to the inversion where massive detrainment takes place. In ECMWF a similar term is also used in the prognostic equation for the cloud fraction, leading to high cloud fractions in the inversion. These high values of the cloud-related parameters occur despite the relatively low humidity, which does not appear to be a very realistic feature (for more on this issue see also Teixeira (2001)).

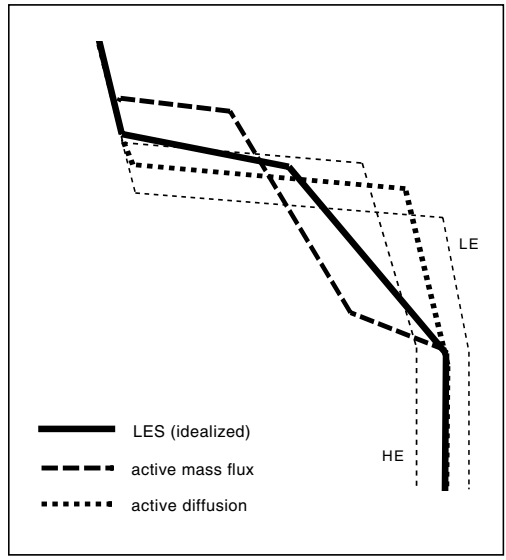

Figure 9. Typical idealized profiles of moisture resulting from models characterized by (too) strong turbulent mixing, and (too) strong mass-flux activity. The thick solid line represents the idealized profile from the large-eddy simulation (LES). The thin lines labelled 'HE' and 'LE' denote an 'active diffusion' case with high entrainment rate and low entrainment rate at cloud top, respectively. The 'active mass-flux' case responds, in a similar way, to cloud-top entrainment.

5. PROGRESS

(*a*) *Synthesis of previous results*

The activity of both mass-flux and turbulence schemes, and their relative strengths, are major issues. To summarize, we have plotted in Fig. 9 two different profiles of total water corresponding to two typical cases of the SCM results. (1) The 'active diffusion' case represents a model with strong diffusive activity (and correspondingly weak, or normal, mass-flux activity). In the cloud layer, profiles are too close to the moist adiabat (too straight). The cloud fraction is, accordingly, too high. The turbulence scheme tends to produce a relatively low inversion with a sharp gradient. (2) The 'active mass-flux' case corresponds to a model with too strong mass-flux activity. In this model too much moisture is taken out of the lower part of the cloud and deposited near the inversion. In this case the cloud fraction tends to peak near the inversion.

(*b*) *Results of updated models*

Based on the findings described above, many participants updated their models with new physics schemes and/or modified their present schemes. Results of some successful updates are described briefly below. It is not our goal to describe and analyse these changes extensively. Merely, we would like to illustrate which types of modification may lead to improved results. Significant improvements were obtained in four models, which are referenced by ECMWF-WST, RACMO-WST, ARPEGE-TKE, and HIRLAM-CLIM. Though there might have been some tuning for the present case in these models, the models are certainly not strongly tuned and the parameters used (e.g. for the w_* closure) are close to what has been reported in literature.

ECMWF-WST uses a new closure of the cloud-base mass flux that is based on the convective velocity scale (Grant 2001)

$$M_{\text{base}} = a w_*, \tag{13}$$

with $a = 0.03$. The closure based on subcloud moist static-energy convergence employed in the reference version gave unrealistically high values of the cloud-base mass flux in the early hours of cloud formation. This is prevented by using Eq. (13). Also the boundary-layer scheme for convective conditions was replaced (Siebesma and Teixeira 2000) and the updraught properties at cloud base were computed from a new parcel method (Jakob and Siebesma 2003).

RACMO-WST also employs the convective velocity-scale closure expressed in Eq. (13), but with a slightly higher value of $a = 0.04$. The main reason for this change is that the moisture-convergence closure used gave rise to a regime transition to higher cloud fractions at the end of the simulation period. In addition, mixing of momentum in the mass-flux scheme was turned off but, at the same time, vertical diffusion was added using

$$K_{\text{mf}} = l_{\text{mf}} M, \tag{14}$$

with $l_{\text{mf}} = 100$ m. The length scale, l_{mf}, was chosen so that about 20–30% of the total flux of q_{t} and θ_{l} in the cloud is due to diffusion and the other part due to the mass flux, as supported by LES results reported by Siebesma *et al.* (2003). One may consider this additional diffusion as representing mixing by the smaller eddies in the cloud; it is done for heat, moisture and momentum.

To improve the numerical stability in ARPEGE-TKE, the diagnostic turbulence closure was replaced by a prognostic TKE-*l* scheme with the Bougeault and Lacarrère (1989) 'parcel' length scale. The moist turbulence scheme was extended by mixing in moist conserved variables, and a non-local term (skewed) was added to Eq. (5). A mass-flux scheme was added, based on the ideas of Kain and Fritsch (1990) and described by Bechtold *et al.* (2001). Chaboureau and Bechtold (2002) and Lopez (2002) have described the new cloud and condensation scheme.

Finally, in HIRLAM-CLIM, the main change was a replacement of the cloud and convection scheme STRACO by a package developed by the Swedish Meteorological and Hydrological Institute's Rossby Climate Modelling Centre, consisting of the Kain and Fritsch (1990) convection scheme and the Rasch and Kristjánsson (1998) cloud/condensation scheme (Unden *et al.* 2002).

Results of these updated schemes are shown in Fig. 10. The time-series of the cloud cover show lower, and more realistic, values below 40% in the models, except ECMWF-WST. The latter shortcoming is caused by the prognostic cloud scheme in which cloud cover is too strongly tied to the (massive) detrainment of the mass-flux scheme. The thermodynamical profiles are significantly improved in all models, as can be seen from the relative-humidity profiles, though HIRLAM-CLIM shows the footprint of too strong mass-flux activity. The wind profiles in RACMO-WST are vastly improved due to deactivation of momentum transport by the mass-flux scheme and the inclusion of additional diffusive momentum transport. In HIRLAM-CLIM there is a trace of numerical instability left.

To illustrate both the activity of the diffusion and the mass-flux scheme, we plotted K_{h} and M at 2130 UTC in Fig. 11. The mass fluxes are of the same order of magnitude, but the different models have rather different shapes; ranging from constant with height (ECMWF-WST), uniformly decreasing with height (RACMO-WST), to first increasing and then decreasing with height in the two models based on Kain and Fritsch (1990)

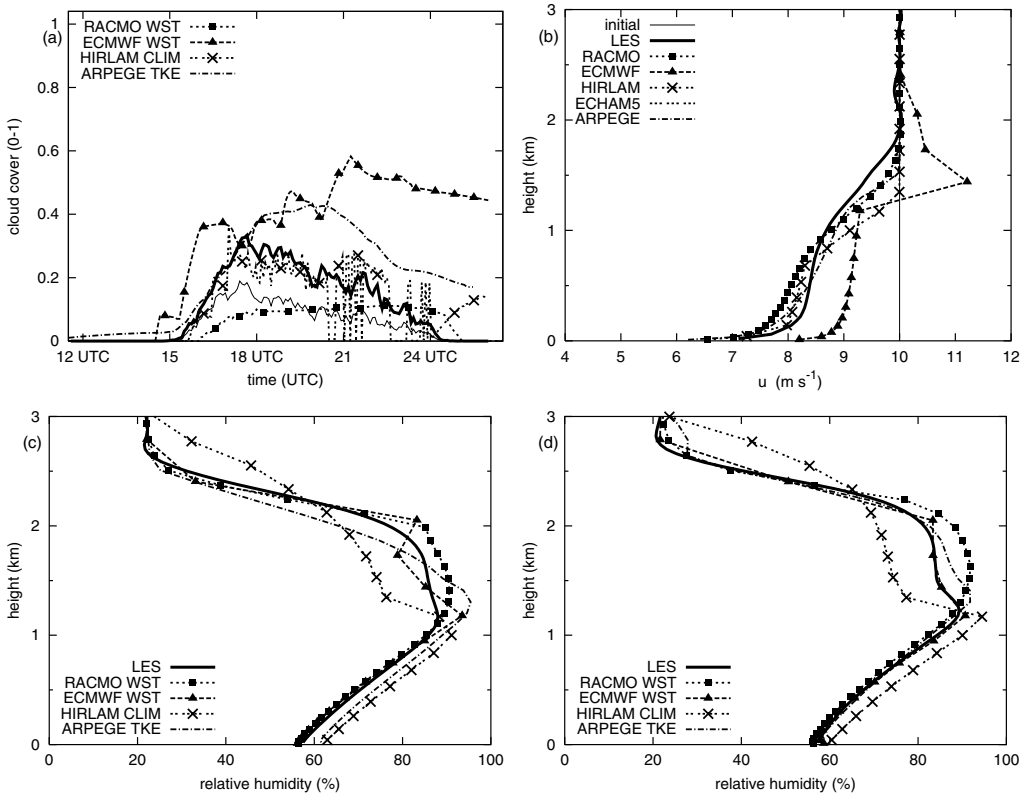

Figure 10. (a) Time-series of cloud cover, (b) profiles of wind, (c) profiles of relative humidity at 2130 UTC and (d) profiles of relative humidity at 0130 UTC in the updated models.

(ARPEGE-TKE and HIRLAM-CLIM). All models have similar quadratic shape profiles of K_h in the subcloud layer, with small values in the cloud layer.

Finally, in ECHAM (results not shown) the change of the cloud-cover scheme from a relative-humidity-based scheme (Sundqvist *et al.* 1989) to a statistical-cloud-cover scheme (Tompkins 2002) vastly improved the onset of cloud formation. However, the convective and turbulent transports still caused a significant moist bias close to the inversion, leading to high cloud amounts.

(*c*) *Resolution dependency*

The results of most models depend strongly on vertical resolution. To illustrate typical model-resolution dependencies we present the results of ECHAM4, METO, RACMO-WST, ARPEGE-TKE at R_{19} and R_{40} resolutions in Fig. 12. In ECHAM4, results of the high-resolution runs are much more contaminated by grid-point noise. The results on R_{19} are reasonable, but the R_{40} results are unacceptable due to instabilities related to the turbulence scheme. In RACMO the results on R_{19} are characterized by a more shallow and moist cloud layer. This is related to the fact that the layer with massive detrainment at cloud top is diagnosed as the whole layer immediately below the first level where the cloud updraught is negatively buoyant. It does not take into account that part of this layer may be in the active buoyant cloud where there should be no massive detrainment. In particular, with low resolution too much moisture is therefore deposited in the active cloud. Results of RACMO-WST obtained with a 50 m grid spacing are

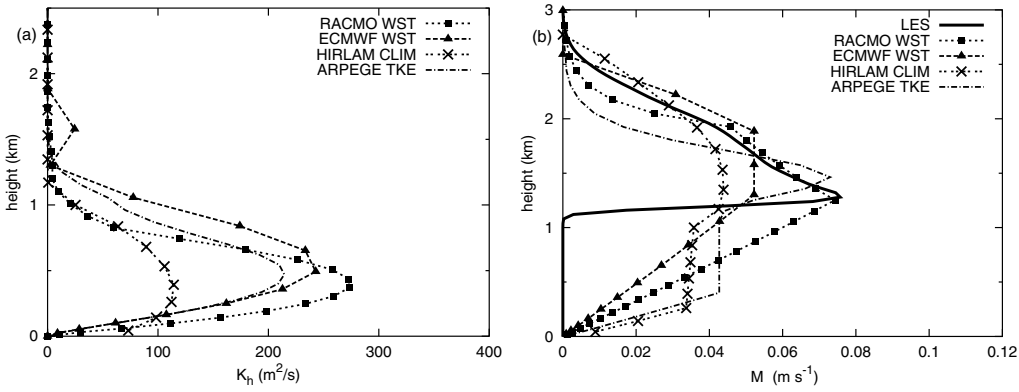

Figure 11. Profiles of (a) eddy-diffusivity and (b) mass-flux at 2130 UTC in the updated models.

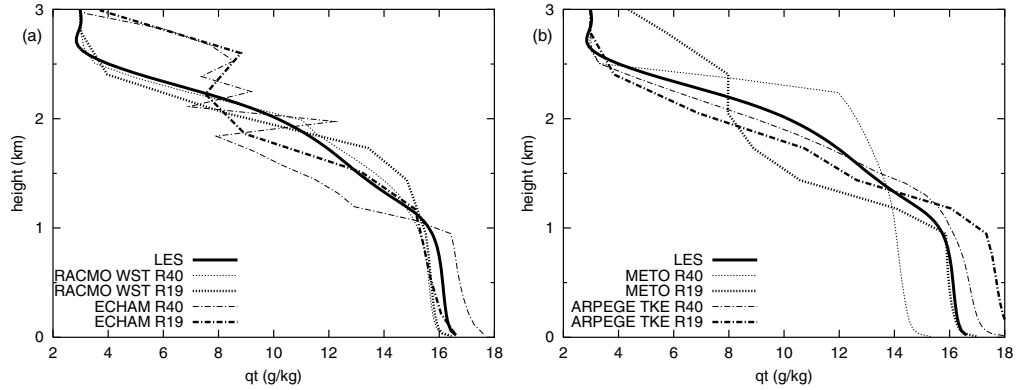

Figure 12. Profiles of total water at 2130 UTC for (a) RACMO-WST and ECHAM, and (b) METO and ARPEGE-TKE on two different vertical resolutions (see text).

almost identical to the R_{40} results, showing that this effect becomes insignificant at R_{40} resolution.

The results of METO and ARPEGE-TKE show rather large sensitivities to vertical resolution. The low-resolution results are considerably more moist in the subcloud layer (1–2 g kg^{-1}), and gradients at cloud base are (much) larger. The latter reflects the weak activity of the turbulence scheme across cloud base (which is unable to moisten the lower part of the cloud layer sufficiently) and/or the strong activity of the mass-flux scheme. In METO the signature of the simulation changes from a typical 'active-diffusion case' at R_{40} to a 'active-mass-flux case' at R_{19} (see Fig. 9). In ARPEGE this effect is also visible, but less pronounced.

It is noted that METO and ECHAM4 perform (somewhat) better on R_{19} resolution. In ECHAM4 the amount of grid-point noise is significantly lower on R_{19} compared with the high-resolution results. In METO the properties of the subcloud layer are close to the LES, but the cloud layer shows the imprint of a too active mass-flux scheme. The results of METO on R_{19} are rather close to the results on the resolution the model is run operationally.

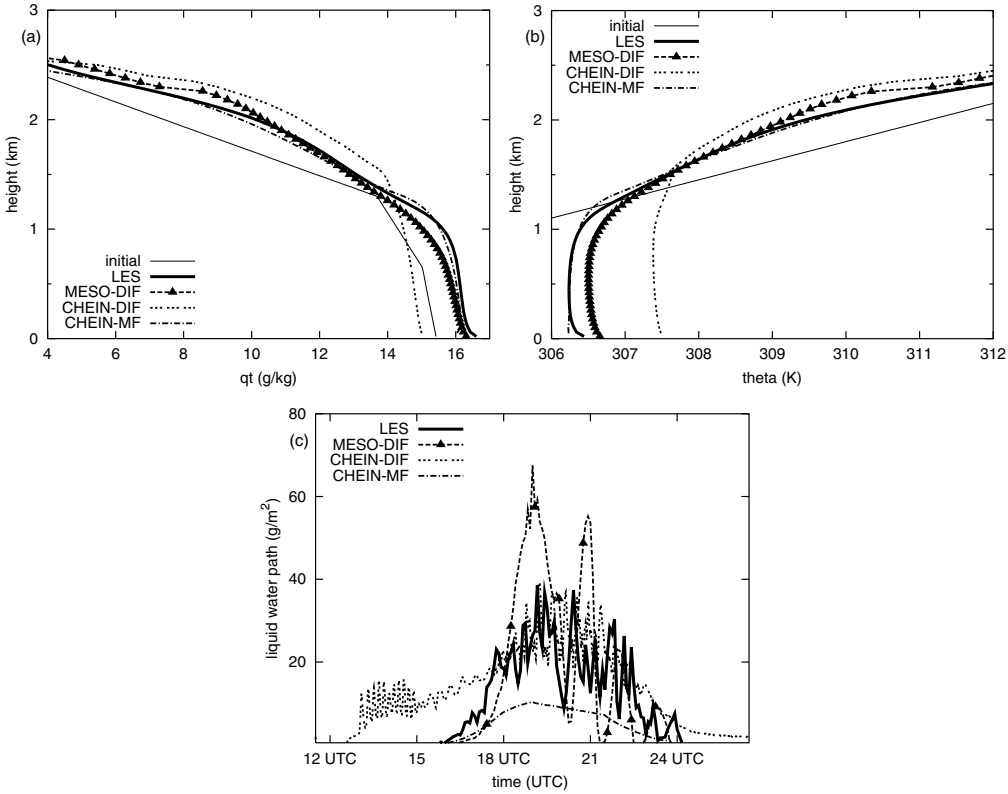

Figure 13. Results of the models based on a unified approach. Shown are the profiles of (a) q_t (g kg^{-1}) and (b) θ (K) at 2130 UTC and (c) the time-series of the cloud liquid-water path (g m^{-2}).

(*d*) *Unified approaches*

Considering the ad-hoc way that turbulent diffusion schemes and convection schemes are coupled, it appears advantageous to use unified approaches to represent fluxes in the cloud and subcloud layers. Therefore, as a bonus, results of three research models based on such an approach are presented.

Two models, MESO-DIF (described by Sanchez and Cuxart (2004)) and CHEIN-DIF (described by Cheinet and Teixeira (2003)), employ a unified approach based on diffusion using a moist TKE-*l* closure. Results in Fig. 13 of these show a reasonable skill in predicting the temperature and moisture profiles, in particular when compared with the results of the operational SCMs (see Fig. 5). On the downside, however, the results are characterized by a rather high level of intermittency in the cloud layer related to the interaction of the moist turbulence scheme with the cloud condensation physics (as discussed in section 4(b)). Also these models tend to create a too sharp inversion, reflecting the fact that a local diffusion scheme is not able to represent the overshoots of the strongest updraughts in the inversion.

CHEIN-MF uses a multi-parcel mass-flux approach (Cheinet 2003). As shown in Fig. 13, the temperature and humidity profiles predicted by CHEIN-MF are very close to the LES results, both in the cloud layer and in the subcloud layer. The fact that the same entraining plume model is used for the unsaturated and the saturated updraughts is thought to explain the consistent treatment of the subcloud-layer and cloud-layer mixing. Timing of the convective activity is very good (see the LWP in Fig. 13(c)). Since

this model is purely diagnostic with respect to the turbulence variables, this suggests that the cloud layer adjusts very rapidly to the surface forcing in our case. Also, the model results turned out to be (much) less sensitive to vertical resolution compared with bulk mass-flux approaches (Cheinet 2003).

6. Discussion

An intercomparison of the diurnal cycle of cumulus convection in different SCMs derived from (semi-) operational models is presented. The SCM results revealed several deficiencies. In general, results are characterized by: too large values of cloud liquid water and cloud cover, strong intermittent behaviour, and unrealistic profiles of temperature and humidity (and wind) in the cloud layer.

The results are analysed in terms of the behaviour of the different parametrization schemes involved: the turbulence schemes, the cumulus convection schemes, and the cloud and condensation schemes. The different models have different causes for their deficiencies. The main causes are (not applying all to any one model):

- Too strong activity of the turbulence scheme in the cloud layer, giving rise to too strongly mixed and, in most cases, too shallow and too moist boundary layers;
- Too strong activity of the mass-flux scheme causing a too dry (warm) lower part of the cloud, and a too moist (cold) upper part—often a (strong) temperature inversion at cloud base is formed, prohibiting any further turbulent transport across cloud base;
- Unrealistic feedback loops between mass-flux activity and (subcloud) turbulence, in particular related to the mass-flux closure;
- Unrealistic transport of momentum in the mass-flux scheme;
- Strong intermittency, mainly caused by the interaction of the (moist) turbulence scheme with the cloud scheme and the convection scheme;
- Too strong dependency of the cloud/condensation scheme on the (massive) detrainment by the mass-flux scheme.

In general, the SCM results could be divided into two different classes. In one class, turbulent activity was too strong and in the other class the mass-flux activity was too strong. Typical, idealized profiles obtained in these classes are shown in Fig. 9. Paradoxically, in both classes too high values of cloud cover and liquid-water content occur; in the first class this is a realistic consequence of the shallow moist boundary layer, and in the second class it is mainly caused by the (unrealistically) strong dependency of cloud liquid water and/or cloud fraction on the detrainment from the mass-flux scheme. In this respect, the closure assumption of the mass-flux scheme plays a crucial role (see also Neggers *et al.* (2004) for the impact of different closure assumptions for the present case).

Due to the large surface forcing, the triggering of convection is not a major issue here. The initialization of convection is determined by the so-called 'trigger-function', which essentially is an explicit rule determining the on and off switching of convection—for example, using the buoyancy of a parcel originating from the surface at the lifting condensation level. However, some of the schemes presented here also trigger convection in a stratocumulus case (Duynkerke *et al.* 2004), showing that, in general, the trigger function is very important.

The dependency of the results on vertical resolution is a major issue. Results of the models do not necessarily converge, or become better, at high resolution. Models tend to suffer from numerical instabilities at higher resolution originating from the turbulence scheme and its interaction with the cloud and condensation scheme, and

with the convection scheme. In addition, the reduced numerical diffusion in (advective) mass-flux schemes at high resolution may degrade the results. Trivially, numerically unstable models do not produce convergent results with higher resolution. Also, hidden resolution dependencies in the code (e.g. in the mass-flux scheme) may come into play. Convergence for RACMO-WST at a resolution of 200 m in the cloud layer has been established. But for the other operational models such convergence could not be proved.

Based on these findings, several SCMs have been updated with new physics packages and/or their present packages have been revised. These new models perform significantly better on this case, though there are some remaining deficiencies. All updated models use a bulk mass-flux approach combined with diffusion in the subcloud layer. For this combination, the following specific recommendations are made:

- use a turbulence scheme based (predominantly) on non-local stability characteristics (e.g. Bougeault and Lacarrère 1989; Lenderink and Holtslag 2004);
- use a mass-flux closure based on the convective velocity scale of the subcloud layer (e.g. Grant 2001);
- use either local diffusion for transport of momentum in the cloud layer, or a mass-flux approach with weak non-local characteristics; that is, with updraught properties that relax strongly to environmental profiles (see also Brown (1999) for more on this issue);
- use a statistically-based cloud scheme, or a prognostic scheme with a weaker (than presently used in many models) dependency on massive detrainment by the mass-flux scheme.

It should be noted that we do not argue that with other (types of) schemes realistic results cannot be obtained; we argue that SCMs that satisfy these points perform reasonably well in the present case.

Summarizing, the paper shows that the present state of cloud modelling has three major sources of error related to: (1) our understanding of the basic physical processes, (2) our understanding of how to couple what we regard as distinct processes, and (3) the numerical implementation of these processes on a grid. In particular, the last two points are considered to be most important. With respect to the second point, multiple mass-flux approaches (such as, for example, has been proposed by Cheinet (2003) and Neggers *et al.* (2002)) are a promising way of achieving a (numerically stable) consistent treatment of subcloud-layer turbulence and cloud mixing.

Acknowledgements

This work benefited greatly from discussions during several EUROCS workshops. In particular, we would like to thank Joan Cuxart, Andreas Chlond, Pedro Miranda, Bjorn Stevens and an anonymous reviewer for their comments on earlier versions of this paper. This study has been made with financial support of the European Union (contract number EVK2-CT-1999-00051).

Appendix A

Model description

The physics packages of the (semi-) operational model are summarized in Table A.1. Some more detailed information is given below.

ARPEGE employs a second-order Mellor and Yamada (1974) turbulence closure with diagnostic TKE. Mixing is done for dry static energy and water vapour only, though the scheme uses a moist formulation for stability (Bougeault 1982). For shallow

TABLE A.1. MODEL DETAILS

Scientists	Model	Diffusion	Convection	Cloud
Marquet	ARPEGE[-TKE][1]	TKEd [TKE]/d [m]	No [KF]	Dc/Dl [Pl]
Siebesma	ECMWF[-WST]	PRO/d	T	Pc/Pl
Mueller (Chlond)	ECHAM4[2]	TKE/m	T	Dc/Pl
Lenderink	RACMO[-WST][3]	TKE/m	T	Dc/Pl
Irons	METO	PRO/m	GR	Dc/Dl
Soares (Miranda)	MESO-NH[4]	TKE/m	KF	Dc/Dl
Olmeda/Calvo	HIRLAM[5]	TKE/d	KUO	Dc/Pl
Jones	HIRLAM-CLIM[5]	TKE/d	KF	Dc/Pl
Sanchez (Cuxart)	MESO-DIF	TKE/m	No	Dc/Dl
Cheinet	CHEIN-DIF	TKE/m	No	Dc/Dl
Cheinet	CHEIN-MF	No	MulMF	Dc/Dl

[..] indicates updated model versions; 'no' signifies that the indicated process is not included.
Column 2: [1]Gibelin and Déqué (2003); [2]Roeckner *et al.* (1996); [3]Lenderink *et al.* (2000); [4]Lafore *et al.* (1998); [5]Unden *et al.* (2002).
Column 3: 'd' mixing in dry variables only; 'm' mixing in moist variables and/or computation stability in moist variables; 'TKE' a prognostic turbulent kinetic energy; 'TKEd' the diagnostic turbulent kinetic energy; 'PRO' a K-profile method.
Column 4: 'KF' Kain and Fritsch (1990); 'T' Tiedtke (1989); 'KUO' Kuo (1974); 'GR' Gregory and Rowntree (1990); 'MulMF' multiple mass flux (Cheinet 2003).
Column 5: 'Pc' prognostic cloud cover; 'Dc' diagnostic cloud cover; 'Pl' prognostic cloud liquid water; 'Dl' diagnostic cloud liquid water.

convection, the mass-flux scheme is inactivated. A statistical cloud scheme (Ricard and Royer 1993) with diagnostic cloud liquid water and cloud fraction is used.

ECHAM4 (Roeckner *et al.* 1996) uses a moist turbulence scheme based on prognostic TKE, with the length-scale formulation based on Louis (1979). The convection scheme is the bulk mass-flux scheme of Tiedtke (1989). The Sundqvist *et al.* (1989) scheme is used for cloud condensation and evaporation. Cloud fraction is based on relative humidity.

RACMO is based on ECHAM4 physics. The length scale in the ECHAM4 turbulence scheme has been replaced in order to improve the behaviour for (moist) convective conditions, as discussed by Lenderink and Holtslag (2004). The cloud fraction is computed by a simple statistical scheme with a link between mass-flux activity and the variance of total water used in the cloud scheme (Lenderink and Siebesma 2000). RACMO uses the Tiedtke (1989) mass-flux scheme, but with modified (increased) entrainment and detrainment coefficients for shallow convection (Siebesma and Holtslag 1996).

ECMWF uses the Louis (1979) scheme for stable conditions and a K-profile method (Troen and Mahrt 1986) for unstable conditions with a prescribed top entrainment rate. The scheme mixes 'dry' variables only (water vapour and dry static energy) and is based on dry formulation for stability. The convection scheme is the Tiedtke (1989) mass-flux scheme. ECMWF uses a fully prognostic cloud scheme with prognostic equations for both cloud fraction and cloud condensate (Tiedtke 1993).

HIRLAM uses a 'dry' TKE-l scheme with the Bougeault and Lacarrère (1989) parcel length-scale formulation (Cuxart *et al.* 2000). The convection and cloud scheme is STRACO (Soft Transition Condensation), which combines a modified Kuo (1974) convection scheme with clouds and condensation based on that of Sundqvist *et al.* (1989). A switch has been introduced to turn off convection smoothly in the full three-dimensional model for horizontal resolutions below 10 km. The present SCM simulations used a 4 km resolution, which means that the convective tendencies are significantly reduced.

METO uses a K-profile method combined with prescribed entrainment rates to compute turbulent fluxes. It is uses a non-local transport term in convective conditions (Holtslag and Boville 1993). It mixes conserved variables and is based on a moist formulation of stability. The Gregory and Rowntree (1990) convection scheme is used, together with a closure bases on w_* (Grant 2001). The entrainment rates are as Grant and Brown (1999). The cloud scheme is diagnostic and is based on relative humidity.

MESO-NH uses a moist turbulence scheme (Cuxart *et al.* 2000) based on the Bougeault and Lacarrère (1989) length scale. The mass-flux scheme used is the Kain and Fritsch (1990) scheme. It uses a statistical cloud scheme based on total-water and liquid-water potential temperature.

REFERENCES

Bechtold, P., Bazile, E., Guichard, F., Mascart, P. and Richard, E. 2001 A mass-flux convection scheme for regional and global models. *Q. J. R. Meteorol. Soc.*, **127,** 869–886

Bougeault, P. 1982 Cloud-ensemble relations based on the gamma probability distribution for the higher-order models of the planetary boundary layer. *J. Atmos. Sci.*, **39,** 2691–2700

Bougeault, P. and Lacarrère, P. 1989 Parameterization of orography-induced turbulence in a meso-beta-scale model. *Mon. Weather Rev.*, **117,** 1872–1890

Brown, A. R. 1999 Large-eddy simulation and parametrization of the effects of shear on shallow cumulus convection. *Boundary-Layer Meteorol.*, **91,** 65–80

Brown, A. R., Cederwall, R. T., Chlond, A., Duynkerke, P. G., Golaz, J.-C., Khairoutdinov, J. M., Lewellen, D. C., Lock, A. P., Macvean, M. K., Moeng, C.-H., Neggers, R. A. J., Siebesma, A. P. and Stevens, B. 2002 Large-eddy simulation of the diurnal cycle of shallow cumulus convection over land. *Q. J. R. Meteorol. Soc.*, **128,** 1075–1094

Browning, K. A. 1993 The GEWEX Cloud System Study (GCSS). *Bull. Amer. Meteorol. Soc.*, **74,** 387–399

Chaboureau, J.-P. and Bechtold, P. 2002 A simple cloud parameterization derived from cloud resolving model data: Diagnostic and prognostic applications. *J. Atmos. Sci.*, **59,** 2362–2372

Cheinet, S. 2003 A multiple mass-flux parameterization for the surface-generated convection. Part 2: Cloudy cores. *J. Atmos. Sci.*, **61,** 1093–1113

Cheinet, S. and Teixeira, J. 2003 A simple formulation for the eddy-diffusivity parameterization of cloudy boundary layers. *Geophy. Res. Lett.*, **30**(18), 1930 doi:10.1029/2003GL017377

Cuijpers, J. W. M. and Bechtold, P. 1995 A simple parameterization of cloud related variables for use in boundary layer models. *J. Atmos. Sci.*, **52,** 2486–2490

Cuijpers, J. W. M. and Duynkerke, P. G. 1993 Large-eddy simulation of trade-wind cumulus clouds. *J. Atmos. Sci.*, **50,** 3894–3908

Cuxart, J., Bougeault, P. and Redelsperger, J.-L. 2000 A turbulence scheme allowing for mesoscale and large-eddy simulations. *Q. J. R. Meteorol. Soc.*, **126,** 1–30

De Roode, S. R. and Duynkerke, P. G. 1997 Observed Lagrangian transition of stratocumulus into cumulus during ASTEX: Mean state and turbulence structure. *J. Atmos. Sci.*, **54,** 2157–2173

Duynkerke, P. G., De Roode, S. R., Van Zanten, M. C., Calvo, J., Cuxart, J., Cheinet, S., Chlond, A., Grenier, H., Jonker, P. J., Köhler, M., Lenderink, G., Lewellen, D., Lappen, C.-L., Lock, A. P., Moeng, C.-H., Müller, F., Olmeda, D., Piriou, J.-M., Sánchez E. and Sednev, I. 2004 Observations and numerical simulations of the diurnal cycle of the EUROCS stratocumulus case. *Q. J. R. Meteorol. Soc.*, **130,** 3269–3296

Gibelin, A.-L. and Déqué, M. 2003 Anthropogenic climate change over the Mediterranean region simulation by a global variable resolution model. *Climate Dyn.*, **20,** 327–339

Grant, A. L. M. 2001 Cloud-base fluxes in the cumulus-capped boundary layer. *Q. J. R. Meteorol. Soc.*, **127,** 407–422

Grant, A. L. M. and Brown, A. R. 1999 A similarity hypothesis for shallow cumulus transports. *Q. J. R. Meteorol. Soc.*, **125,** 1913–1936

Gregory, D. and Rowntree, P. R. 1990 A mass-flux convection scheme with representation of cloud ensemble characteristics and stability-dependent closure. *Mon. Weather Rev.*, **118,** 1483–1506

Holtslag, A. A. M. and Boville, B. A. 1993 Local versus nonlocal boundary-layer diffusion in a global climate model. *J. Climate*, **6,** 1825–1842

Holtslag, A. A. M. and Moeng, C.-H. 1991 Eddy diffusivity and countergradient transport in the convective atmospheric boundary layer. *J. Atmos. Sci.*, **48,** 1690–1698

Jakob, C. and Siebesma, A. P. 2003 A new subcloud model for mass-flux convection schemes: Influence on triggering, updraft properties and model climate. *Mon. Weather Rev.*, **131,** 2765–2778

Kain, J. S. and Fritsch, J. M. 1990 A one-dimensional entraining/detraining plume model and its application in convective parameterization. *J. Atmos. Sci.*, **47,** 2784–2802

Kuo, H. L. 1974 Further Studies of the parameterization of the influence of cumulus convection on large-scale flow. *J. Atmos. Sci.*, **31,** 1232–1240

Lafore, J.-P., Stein, J., Asensio, N., Bougeault, P., Ducrocq, V., Duron, J., Fischer, C., Hereil, P., Marcart, P., Pinty, J.-P., Redelsperger, J.-L., Richard, E. and Vila-Guerau de Arellano, J. 1998 The Meso-NH atmospheric simulation system. Part 1: Adiabatic formulation and control simulations. *Ann. Geophys.*, **16,** 90–109

Lenderink, G. and Holtslag, A. A. M. 2004 An updated length-scale formulation for turbulent mixing in clear and cloudy boundary layers. *Q. J. R. Meteorol. Soc.*, **130,** 3405–3427

Lenderink, G. and Siebesma, A. P. 2000 'Combining the massflux approach with a statistical cloud schemes'. Pp. 66–69 in Proceedings of the 14th symposium on boundary layers and turbulence, Aspen, USA. American Meteorological Society, Boston, USA

Lenderink, G. and van Meijgaard, E. 2001 Impacts of cloud and turbulence schemes on integrated water vapor: Comparison between model predictions and GPS measurements. *Meteorol. Atmos. Phys.*, **77,** 131–144

Lenderink, G., van Meijgaard, E. and Holtslag, A. A. M. 2000 Evaluation of the ECHAM4 cloud-turbulence scheme for stratocumulus. *Meteorol. Zeit.*, **9,** 41–47

Lopez, P. 2002 Implementation and validation of a new prognostic large-scale cloud and precipitation scheme for climate and data-assimilation purposes. *Q. J. R. Meteorol. Soc.*, **128,** 229–258

Louis, J. F. 1979 A parametric model of vertical fluxes in the atmosphere. *Boundary-Layer Meteorol.*, **17,** 187–202

Mellor, G. L. and Yamada, T. 1974 A hierarchy of turbulence closure models for planetary boundary layers. *J. Atmos. Sci.*, **31,** 1791–1806

Neggers, R. A. J., Siebesma, A. P. and Jonker, H. J. J. 2002 A multiparcel model for shallow cumulus convection. *J. Atmos. Sci.*, **59,** 1655–1668

Neggers, R. A. J., Siebesma, A. P., Lenderink, G. and Holtslag, A. A. M. 2004 An evaluation of mass flux closures for diurnal cycles of shallow Cumulus. *Mon. Weather Rev.*, (in press)

Rasch, P. J. and Kristjánsson, J. E. 1998 A comparison of the CCM3 model climate using diagnosed and predicted condensate parameterizations. *J. Climatol.*, **11,** 1587–1614

Ricard, J. L. and Royer, J. F. 1993 A statistical cloud scheme for use in an AGCM. *Ann. Geophys.*, **11,** 1095–1115

Roeckner, E., Bengtsson, L., Christoph, M., Claussen, M., Dumenil, L., Esch, M., Giorgetta, M., Schlese, U. and Schulzweida, U. 1996 'The atmospheric general circulation model ECHAM-4: Model description and simulation of present-day climate'. Tech. Rep. 218, Max-Planck-Institut für Meteorologie, Bundesstrasse 55, D-20146 Hamburg, Germany

Sánchez, E. and Cuxart, J. 2004 A buoyancy-based mixing-length proposal for cloudy boundary layers. *Q. J. R. Meteorol. Soc.*, **130,** 3385–3404

Siebesma, A. P. and Cuijpers, J. W. M. 1995 Evaluation of parametric assumptions for shallow cumulus convection. *J. Atmos. Sci.*, **52,** 650–666

Siebesma, A. P. and Holtslag, A. A. M. 1996 Model impacts of entrainment and detrainment rates in shallow cumulus convection. *J. Atmos. Sci.*, **53,** 2354–2364

Siebesma, A. P. and Teixeira, J. 2000 'An advection-diffusion scheme for the convective boundary layer, description and 1d-results'. Pp. 133–136 in Proceedings of the 14th symposium on boundary layers and turbulence, Aspen, USA. American Meteorological Society, Boston, USA

Siebesma, A. P., Bretherton, C. S., Brown, A., Chlond, A., Cuxart, J., Duynkerke, P. G., Jiang, H., Khairoutdinov, M., Lewellen, D., Moeng, C.-H., Sanchez, E., Stevens, B. and Stevens, D. E. 2003 A large eddy simulation intercomparison study of shallow cumulus convection. *J. Atmos. Sci.*, **60,** 1201–1219

Stevens, B. 2000 Quasi-steady analysis of a PBL model with an eddy-diffusivity profile and non-local fluxes. *Mon. Weather Rev.*, **128,** 824–836

Stevens, B., Ackerman, A. S., Albrecht, B. A., Brown, A. R., Chlond, A., Cuxart, J., Duynkerke, P. G., Lewellen, D. C., Macvean, M. K., Neggers, R. A. J., Sanchez, E., Siebesma, A. P. and Stevens, D. E. 2001 Simulations of trade-wind cumuli under a strong inversion. *J. Atmos. Sci.*, **58,** 1870–1891

Sundqvist, H., Berge, E. and Kristjansson, J. E. 1989 Condensation and cloud parameterization studies with a mesoscale numerical prediction model. *Mon. Weather Rev.*, **117,** 1641–1657

Teixeira, J. 1999 'The impact of increased boundary layer vertical resolution on the ECMWF forecast system'. Tech. Rep. 268, European Centre for Medium-Range Weather Forecasts, Shinfield Park, RG2 9AX Reading, UK

2001 Cloud fraction and relative humidity in a prognostic cloud fraction scheme. *Mon. Weather Rev.*, **129,** 1750–1753

Tiedtke, M. 1989 A comprehensive mass flux scheme for cumulus parameterization in large-scale models. *Mon. Weather Rev,*, **177,** 1779–1800

1993 Representation of clouds in large-scale models. *Mon. Weather Rev.*, **121,** 3040–3061

Tompkins, A. 2002 A prognostic parameterization for the subgrid-scale variability of water vapor and clouds in large-scale models and its use to diagnose cloud cover. *J. Atmos. Sci.*, **59,** 1917–1942

Troen, I. and Mahrt, L. 1986 A simple model of the atmospheric boundary layer: sensitivity to surface evaporation. *Boundary-Layer Meteorol.*, **37,** 129–148

Undén, P., Rontu, L., Järvinen, H., Lynch, P., Calvo, J., Cats, G., Cuxart, J., Eerola, K., Fortelius, C., Garcia-Moya, J. A., Jones, C., Lenderink, G., McDonald, A., McGrath, R., Navascues, B., Nielsen, N. W., Ødegaard, V., Rodrigues, E., Rummukainen, M., Rõõm, R., Sattler, K., Sass, B. H., Savijärvi, H., Schreur, B. W., Sigg, R., The, H. and Tijm, A. 2002 'HIRLAM-5 scientific documentation.' Tech. Rep., Swedish Meteorological and Hydrological Institute, S-601 76 Norrköping, Sweden

Van Salzen, K. and McFarlane, N. A. 2002 Parameterization of the bulk effects of lateral and cloud-top entrainment in transient shallow cumulus clouds. *J. Atmos. Sci.*, **59,** 1405–1430